JOURNAL OF CATALYSIS 148, 119–124 (1994)

Iron–Aluminum Cluster Catalysts Obtained by Alkoxy Synthesis

2. Iron–Aluminum Catalysts for CO Hydrogenation: Selectivity–Structure Relation

Yu. V. Maksimov,*[,1] M. V. Tsodikov,† O. V. Bukhtenko,† O. G. Ellert,‡ and V. V. Matveev*

*Institute of Chemical Physics, Russian Academy of Sciences, Kosygina ul., 4, Moscow 117977, Russia; †Institute of Petrochemical Synthesis, Russian Academy of Sciences, Leninsky pr., 29, Moscow 117912, Russia; and ‡Institute of General and Inorganic Chemistry, Russian Academy of Sciences, Leninsky pr., 31, Moscow 117912, Russia

Received March 17, 1993; revised October 18, 1993

A series of iron-containing catalysts with 2.5 mass% Fe (A), 5.5–8.0 mass% Fe (B), 5.5–8.0 mass% Fe + 0.2 mass% Zr (B–Zr), and 15.0–20.0 mass% Fe (C) was obtained from gels produced by alkoxy synthesis and treated either under H_2 (400°C) or successively in air (500°C) and under H_2 (400°C). The catalysts were tested in CO hydrogenation (T = 350°C, P = 18 MPa, CO/H_2 = 1) and studied by *in situ* Mössbauer spectroscopic and magnetic susceptibility measurements. Depending on the Fe loading and activation procedure, the catalysts showed more or less selectivity, S, in C_1–C_3–Ph and C_4–C_8–Ph production. Catalysts A and B, treated by H_2, yielded C_1–C_3–Ph with $S \approx 48\%$ and traces of C_4–C_8–Ph. When successively treated with O_2 and H_2, catalysts A and B markedly lost C_1–C_3–Ph selectivity ($S \approx 30\%$) with increasing $S(C_4$–C_8–Ph) to ≈8–9%. Catalyst B–Zr showed the highest selectivity ($S(C_1$–C_3–Ph), ≈ 52%, even after two-step activation. Independent of the activation procedure, catalyst C showed no selectivity at all. The formation of small ($d \approx 3$ nm) carbide clusters Fe_xC and χ-Fe_5C_2 was shown to be a crucial point for process selectivity. No metallic iron phase was observed in selective catalysts. The most selective B–Zr catalyst revealed small amounts of Fe_xC carbide along with high-spin Fe^{3+} and Fe^{2+} in a γ-$Al_{2-x-y}Fe_xZr_yO_3$ matrix. The presence of Zr causes a stabilization effect, inhibiting the loss of lattice oxygen and favoring the reaction of active carbon (C_i) with iron intermediates. The participation of anion vacancies and "oxidic" carbon in selective catalysis is discussed.

INTRODUCTION

The creation of multicomponent catalysts and ceramics motivates the search for new energy- and material-saving methods of preparation. Along with traditional preparation by wet technology, impregnation, coprecipitation, etc., the immobilization and destruction of metallic complexes on the surface of inorganic supports provide an effective new technique for obtaining cluster-derived systems (1–4).

[1] To whom correspondence should be addressed.

Previously, we reported on selective catalysts obtained by the reaction of mononuclear and binuclear carbonyl complexes with the surface of activated γ-Al_2O_3 (5–7). Sol–gel technology—in particular, alkoxy synthesis—allows us to prepare cluster-derived catalysts, adsorbents, ceramics, etc., by the use of Al_2O_3, SiO_2, TiO_2, ZrO_2, or mixtures thereof as host matrixes and Y, Co, Ni, Fe, etc., as additives (8–10). In fact, alumina-supported catalysts for CO hydrogenation, highly selective in alkylaromatic production, have been recently obtained by the reaction of β-diketonates of iron, cobalt, and nickel with the hydrolysate of aluminum alkoxide (8, 9). After appropriate activation, the powdered iron–aluminum catalysts were characterized by a surface area of ca. 300 m^2/g and a transition metal loading of 1–20 mass%.

In previous communications we reported on supported oxide clusters obtained by alkoxy synthesis and effective in low-temperature hexadecane liquid-phase oxidation (11, 12). This work deals with iron-aluminum cluster catalysts obtained in the same way which are highly selective in alkylaromatic production from CO and H_2. Special attention has been given to elucidating the relation between structural peculiarities of the cluster-derived system and process selectivity. Structural studies were performed by Mössbauer spectroscopy and magnetic susceptibility methods; most of the data were taken by *in situ* measurements.

METHODS

Iron–aluminum gels with iron loadings of 1.3–14.0 mass% were synthesized by the reaction of $Fe(acac)_3$ with the hydrolysate of $Al(OR)_3$ ($R = i - C_3H_7$) as reported in (11). Complex iron–zirconium gel (Fe, 4.5 mass%; Zr, 0.2 mass%) was obtained by the use of an appropriate mixture of $Zr(acac)_4$ and $Fe(acac)_3$ by the same reaction.

Initial gels were activated in two different fashions: (i) under H_2 (400°C, 1 atm, 4 h, denoted H_2); (ii) in air (500°C,

0021-9517/94 $6.00

1 atm, 4 h) and then under H_2 (400°C, 1 atm, 4 h, denoted O_2, H_2).

The treatment in H_2 was carried out in a quartz tube under hydrogen flow. Annealing in air was done in a muffle supplied with a thermoregulator. After activation the sample cell was sealed under H_2 flow and replaced for structural studies. DTG data showed that after activation the weight of powdered samples diminished by 45–50% due to evolution of water and organic fragments. At the end, the catalysts contained 2.5 (A), 5.5–8.0 (B, B–Zr), and 15.0–20.0 (C) mass% Fe, respectively.

Synthesis of organic compounds from CO and H_2 was performed in a reactor of periodic action made of stainless steel, using a stirring device. The reactor was heated by a thermocontrolled oven and had a volume of 250 cm^3. First the reactor was loaded with a fixed amount of catalyst in Ar. Then 50 cm^3 of *n*-heptane (chemical purity) and syn-gas (CO/H_2 = 1) were fed into the reactor. The synthesis was carried out at T = 350°C and P = 18 MPa. The duration of each run was ≈30 h. Gas consumption was measured with a calibrated manometer, while the syn-gas loss was replaced by the use of a special volume kept under high pressure. After each run the reactor was cooled to 25°C under syn-gas; the catalyst was removed and placed in special cells under Ar for structural studies.

Gases were analyzed chromatographically: hydrocarbons C_1–C_6 on a column with SKWALANE/α-Al_2O_3 and a flame detector; CO, CO_2, and CH_4 on a column with activated charcoal and a catarometer. Liquids were first separated from *n*-heptane and then analyzed by chromatographic mass spectrometry on LKB and BIOCHROM thermoprogrammable devices. Capillary columns (l = 50 m, d = 0.25 mm) and phases OY-17 and SE-30 were used.

Magnetic susceptibility measurements were performed with the Faraday balance method at 77 and 300 K in magnetic fields 0–12 kOe. Glass cells and tablets were used for *in situ* measurements.

The Mössbauer spectra were recorded and fitted as in (11). To study intermediates an absorption Mössbauer *in situ* cell made of Pyrex glass (6) and thin tablets prepared and kept in Ar were used. To obtain the tablets the iron-containing powders (grain size ≈0.05 mm) were mixed with small amounts of binding material (Apiezon) in a gas control atmosphere. It was shown that *in situ* samples did not suffer oxidation during storage. It should be noted that the unfavorable geometry of the glass *in situ* cell gave a sensitivity 2–2.5 lower than that of the tablets. A sensitivity increase was achieved by enrichment of the sample with 20–30% ^{57}Fe.

RESULTS AND DISCUSSION

Selectivity in CO Hydrogenation

Data on testing of iron-containing catalysts in CO hydrogenation are displayed in Table 1. It is seen that the increase of iron content to ≈8 mass% produces growth in the overall activity (W) and in the extent of CO conversion. It is of great importance that A and B catalysts showed high selectivity of alkylaromatic production, $S(C_1$–C_8–Ph), whereas the type of preliminary treatment strongly affected the catalytic properties. In contrast to activation of A and B by only H_2, the two-step treatment (O_2, H_2) led to a decrease in both $S(C_1$–C_3–Ph) and overall activity. Simultaneously, the $S(C_4$–C_8–Ph) increased. The zirconium-modified catalyst B–Zr showed the highest selectivity in C_1–C_3–Ph production even after

TABLE 1

Overall Activity and Product Distribution over Catalysts A, B, B–Zr, and C

Catalyst	Iron load %	Activation[a]	W^b (μmol/ g · min)	Liquid products				Gas products	
				C_1–C_3–Ph	C_4–C_8–Ph	Alkenes	Alkanes	C_1–C_5	CO_2
A	2.5	(H_2)	0.6	48.3	tr.[c]	tr.	tr.	2.5	49.2
		(O_2), (H_2)	0.4	27.3	6.2	tr.	tr.	2.0	64.0
	5.6	(H_2)	1.8	46.0	tr.	tr.	tr.	3.0	51.0
		(O_2), (H_2)	1.1	30.0	8.0	tr.	tr.	3.5	58.5
B	8.0	(H_2)	3.5	48.0	tr.	tr.	tr.	3.2	48.8
		(O_2), (H_2)	1.6	30.0	11.8	tr.	tr.	3.5	54.7
	15.0	(H_2)	2.5	–	2.0	6.0	20.0	8.0	64.0
		(O_2), (H_2)	1.7	–	—	3.0	22.0	10.0	65.0
C	20.0	(H_2)	1.4	—	—	5.0	21.0	8.4	65.6
		(O_2), (H_2)	1.1	—	—	2.0	20.0	11.0	67.0
B–Zr	8.0 (Zr = 0.4)	(O_2), (H_2)	0.7	52.0	tr.	tr.	tr.	3.0	45.0

[a] (H_2) = H_2, 400C; (O_2), (H_2) = O_2, 500C, H_2, 400C.
[b] Rate of CO conversion.
[c] Trace amounts.

two-step activation. C catalysts were not selective independent of the fashion of their activation. Thus, regardless of its nature, selectivity is readily destroyed by augmentation of total iron loading. As all catalysts possess practically the same specific surface area ($S \approx 380$–400 m^2/g), one can see the strong relation between catalytic properties and the nature of iron-containing centers.

Structural Data

According to X-ray data, all iron-containing catalysts, both activated and tested in CO hydrogenation, remained X-ray amorphous. There were no diffraction patterns arising from iron-containing species, except the amorphous halo from γ-Al_2O_3, which is the host matrix of created catalysts.

1. One-Step Activated Catalysts. Mössbauer data on the structural rearrangement of iron-containing gel B after activation in H_2 at 400 C and testing in synthesis in CO and H_2 are shown in Fig. 1. Similar data were obtained for A subjected to the same activation.

Two main features are typical of iron-containing gels A and B after the reduction. First, the quadrupole splitting of the high-spin complex of Fe^{3+} (QS = 1.22 ± 0.05 mm/s) tends to grow after activation, as for the initial gel (QS = 0.7–0.8 mm/s) (Figs. 1a and 1b). The same growth was observed in (12) after O_2 treatment at 500°C and may be caused by the transformation of substituted boehmite into amorphous γ-$Al_{2-x}Fe_xO_3$. In fact, iron seems to have a preference for the octahedral position when replacing aluminum in the γ-Al_2O_3 spinel framework (13). Small size and lattice disorder in alternating stackings may cause essential axial distortion of FeO_6 local polyhedra. The decrease in QS to QS ≈ 0.8–0.9 mm/s after CO hydrogenation (Fig. 1c) seems to provide evidence of small superparamagnetic cluster formation (see below) with Fe–O–Fe superexchange interaction.

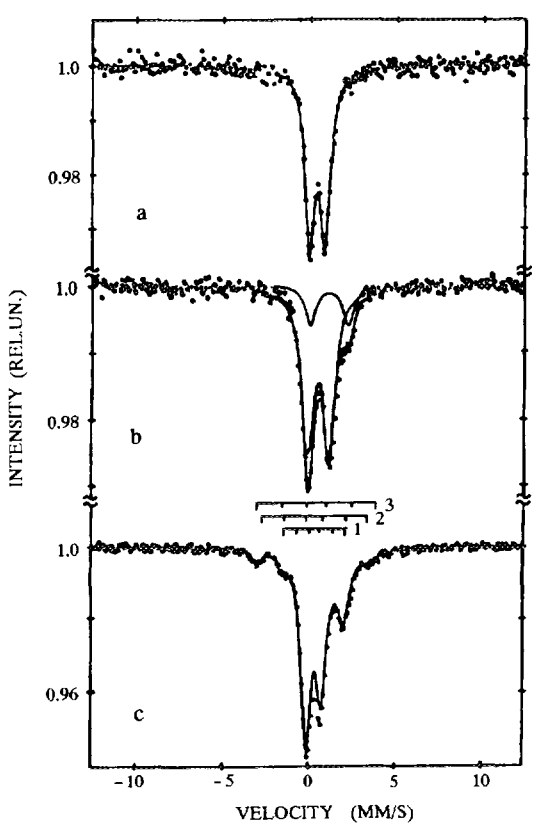

FIG. 1. Mössbauer spectra (T = 300 K) of catalyst B activated by H_2. (a) Gel, (b) gel after activation, (c) gel after activation and CO hydrogenation.

Next, we discuss the presence of high-spin octahedral complexes of Fe^{2+} ions with IS = 0.95–1.1 mm/s and QS = 1.8–2.1 mm/s (Figs. 1b and 1c). The parameters of Fe^{2+} in mixed spinel, obtained by ceramic technology (IS = 1.2–1.4 mm/s, QS = 1.1–2.2 mm/s) (14), are different, thus showing an increased extent of the covalency effect in the catalyst that may favor lattice oxygen mobility (15).

In addition to Fe^{3+} and Fe^{2+} ions in high-spin states, the catalytically active sample contains ≈10% iron carbide, most probably χ-carbide with three nonequivalent sublattices (Fig. 1c, bars 1–3; Table 2) (15). So the active catalyst is heterogeneously composed of iron carbide and iron-substituted spinel (γ-$Al_{2-x}Fe_xO_3$) with a clearcut interface. No clusters of α-iron were detected in either A or B catalysts, even in the samples enriched by ^{57}Fe.

Magnetic data for A, B, B–Zr, and C catalysts are collected in Fig. 2. The remarkable nonlinearity of $\chi(H)$ and $M(H)$ is seen even for sample A, treated with only H_2. The $\chi(H)$ and MS data for catalytically active sample B show the presence of a group of magnetically ordered clusters of χ-Fe_2C_5 (Figs. 1 and 2) with mean size $\langle d \rangle$ = 3 ± 0.5 nm. It is noteworthy that in reduced sample B no ferromagnetic clusters were revealed by Mössbauer spectroscopy (Fig. 1b), but they were easily detected by measurements of $\chi(H)$ (Fig. 2). One may assume the presence of small metallic clusters with relative content ≈0.1%, which is beyond the analytical sensitivity of MS.

The structural peculiarities of catalyst C treated by H_2 differ dramatically from those of A and B. After reduction, the essential parts of initial gel C have been transformed into α-Fe (≈46%) and high-spin complexes of Fe^{3+} (≈29%) and Fe^{2+} (≈25%) in the γ-$Al_{2-x}Fe_xO_3$ matrix. The low-temperature Mössbauer data for initial gel C clearly indicated the presence of small ferrimagnetic spinel clusters (11). Thus, in clusters, the reducibility of ferric or ferrous ions is higher than that of the γ-Al_2O_3 matrix. As a result, catalyst C is the most reduced: the total content of Fe^{2+} and χ-Fe_5C_2 exceeds 80% (Table 2), which correlates with the complete loss of selectivity in alkylaromatic production (Table 1). The analysis of χ(H) and absolute values of χ (Fig. 2) strongly supports the MS measurements.

TABLE 2

MS Data for Catalysts A, B, B–Zr, and C after CO Hydrogenation

Catalyst	Activation	Fe^{3+} IS (mm/s)	Fe^{3+} QS (mm/s)	Fe^{3+} % ±3	Fe^{2+} IS (mm/s)	Fe^{2+} QS (mm/s)	Fe^{2+} % ±3	α-Fe % ±3	χ-Fe_5C_2 % ±3	$Fe_3O_{4+\delta}$ magnetic % ±3
A	H_2, 400C	0.40	0.90	58	1.10	1.80	42	—	traces[a]	—
B	H_2, 400C	0.32	0.89	56	0.96	2.09	34	—	≈10	—
	O_2, 500C; H_2, 400C	0.32	0.78	35	0.92	2.03	23	—	42	traces
C	H_2, 400C	0.30	0.76	16	0.91	1.87	64		20	—
	O_2, 500C; H_2, 400C	0.31	0.65	15	0.90	1.85	34	—	43	≈8
B–Zr	O_2, 500C; H_2, 400C	0.34	0.87	59	1.07	2.13	38	—	≈3[a]	—

[a] Metastable Fe_xC; accuracy of IS, QS ± 0.03 mm/s.

2. Two-step activated catalysts. Part of the initial gel B after O_2 treatment has been transformed into magnetite-like clusters with $H_{in}(1) \approx 495$ kOe and $H_{in}(2) \approx 460$ kOe (Fig. 3b, bars 1, 2). The central doublet (IS = 0.31 ± 0.05 mm/s, QS = 1.15 ± 0.05 mm/s) again belongs to octahedral high-spin Fe^{3+} complexes distributed throughout the γ-$Al_{2-x}Fe_xO_3$ matrix in a random fashion.

After subsequent H_2 treatment, a small part of the iron was converted to an Fe^{2+} compound of unknown structure with $H_{in} \approx 434$ kOe, IS ≈ 0.85 mm/s, and QS ≈ 0.05 mm/s (Fig. 3c, bar 3). The γ-$Al_{2-x}Fe_xO_3$ host matrix contains Fe^{3+} and Fe^{2+}, both in a high-spin state.

The clearcut carbide/oxide interface is present after CO hydrogenation (Fig. 3d, bars 4–6; Table 2). The compari-

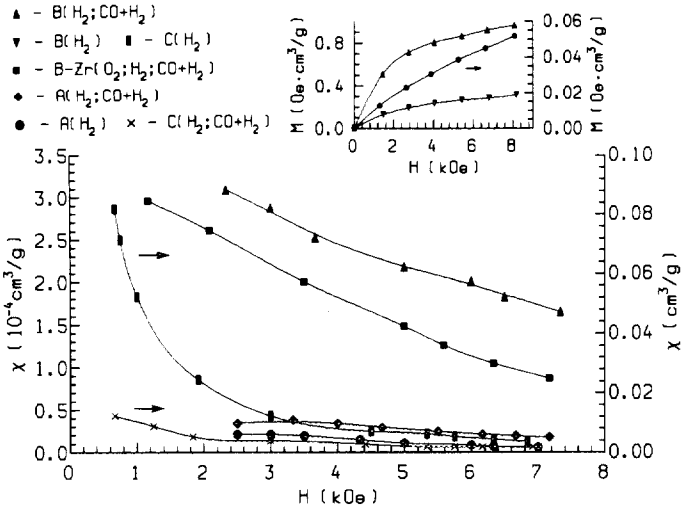

FIG. 2. Magnetic susceptibility (T = 300 K) vs external magnetic field. X axis, external field, H (kOe). Y axis (left) magnetic susceptibility, $\chi \cdot 10^{-4}$ (cm^3/g). Y axis (right), magnetic susceptibility, χ (cm^3/g). Insert: Magnetization vs external field. X axis, H, kOe. Y axis (left), M (Oe · cm^3/g). Y axis (right), M (Oe · cm^3/g).

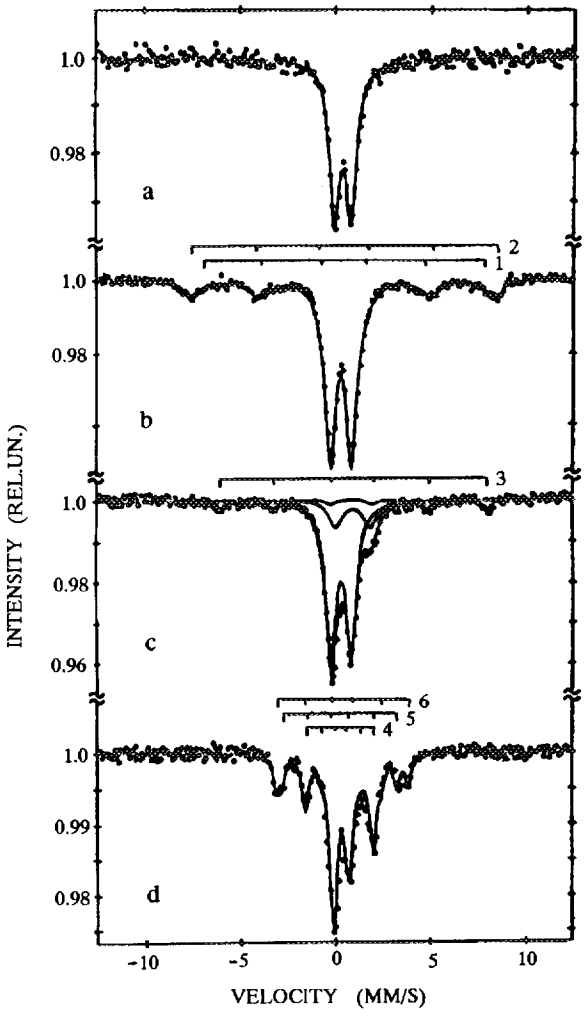

FIG. 3. Mössbauer spectra (T = 300 K) of catalyst B activated by O_2 and H_2. (a) Gel, (b) gel after O_2 activation, (c) (b) after H_2 activation, (d) (c) after CO hydrogenation.

son of total reduction (Fe^{2+} + carbide) of catalyst B after one- and two-step activation shows that the less the reduction of the catalyst, the higher the selectivity of alkylaromatic production.

A room temperature (RT) spectrum of sample C treated by O_2 showed qualitatively the same result as B. According to (12), at T = 4.2 K, i.e., below or near the blocking temperature, ≈70–80% of the total spectral area of catalyst C was converted to HFS lines arising from magnetic clusters with some size distribution. For catalyst B this value does not exceed 10–15%. As sample C is much less uniform than B, treatment by H_2 resulted in ≈87% of α-Fe, ≈10% of Fe^{2+}, and ≈3% of Fe^{3+}. Thus, the total reduction of catalyst C after CO hydrogenation was among the highest (≈77%, Table 2).

Consider now the structural peculiarities of the most selective catalyst, B–Zr. The RT spectrum of the initial gel (Fig. 4a) is similar to that typical of A, B, and C gels. In contrast to B, after (O_2, H_2) treatment B–Zr shows only "paramagnetic" high-spin Fe^{3+} (IS = 0.36 mm/s, QS = 1.55 mm/s; rel.content ≈82%) and high-spin Fe^{2+} (IS = 1.02 mm/s, QS = 1.84 mm/s; rel.content ≈18%), both in the γ-Al_{2-x-y} $Fe_xZr_yO_3$ lattice (Fig. 4b). The total reduction of B–Zr is similar to that of samples A and B after one-step activation (see above). Thus, the modification by zirconium results in at least two effects. First, as QS (B–Zr) > QS(B), axial distortion of the FeO_6 polyhedron clearly increases. This seems obvious, because the ionic radius of Zr^{4+} exceeds the corresponding value for Al^{3+} ($r(Zr^{4+})$ = 0.087 nm; $r(Al^{3+})$ = 0.053 nm and 0.067 nm for 4- and 6-fold coordinated Al^{3+}, respectively). Thus, the substitution of Zr for Al may disturb the local symmetry of cations and change the MS parameters of Fe^{3+}. Second, as even after two-step activation no magnetic hyperfine structure lines appeared in the spectrum (Fig. 4b), the presence of Zr seems to inhibit both lattice oxygen mobility and magnetic cluster formation. Moreover, the ≈0.2 Fe^{2+}/Fe^{3+} ratio in B–Zr does not exceed the corresponding value in catalyst B treated only with H_2. It should be noted that the Fe^{2+}/Fe^{3+} ratio itself may be of great use for tentative estimation of the reducibility of the mixed spinel. In fact, if lattaice oxygen mobility, anion vacancy formation, vacancy ionization, and electron trapping by Fe^{3+} may be written (as in [15, 16])

$$O_L \rightleftarrows V_L + \tfrac{1}{2}O_2, \quad [1]$$

$$O_L + H_2 \rightleftarrows V_L + H_2O, \quad [2]$$

$$V_L \rightleftarrows V_L^+ + e^-, \quad [3]$$

$$Fe^{3+} + e^- \rightleftarrows Fe^{2+}, \quad [4]$$

where O_L is lattice oxygen, V_L is an anion vacancy, and V_L is an ionized vacancy, then at some fixed catalyst treatment, the stronger the *Me*–O bond in the lattice, the lower the Fe^{2+}/Fe^{3+} ratio.

The RT spectrum of the B–Zr catalyst after CO hydrogenation is shown in Fig. 4c. The majority of the resonance absorption is again from "paramagnetic" signals from Fe^{3+} and Fe^{2+} ions with Fe^{2+}/Fe^{3+} = 0.67 (T = 300 K), 0.64 (T = 77 K), and 0.61 (T = 4.2 K), respectively. At T = 4.2 K the intensities of paramagnetic doublets decreased while a broad bag-shaped resonance absorption (≈41% of total spectral area) along with poorly resolved HFS lines (≈8%) appeared in the spectrum. The latter two may arise from the spinal clusters of different sizes, with a maximum value of H_{in} ≈ 460 ± 15 kOe obtained for the largest from the hyperfine field distribution function [11]. Thus, the oxide matrix of the B–Zr catalyst consists of small oxide clusters with $\langle d \rangle$ ≈ 3–7 nm and Fe^{3+} and Fe^{2+} ions in the γ-$Al_{2-x-y}Fe_xZr_yO_3$ matrix. Along with intensive "paramagnetic" signals a new magnetic hyperfine structure with a relative content of ≈3% (300 K) and ≈5% (77 K) may be seen in the spectrum (Fig. 4c, bar 1). Its parameters H_{in} (300 K) ≈ 216 kOe and H_{in} (77 K) ≈ 264 kOe are very close to those for Fe_xC

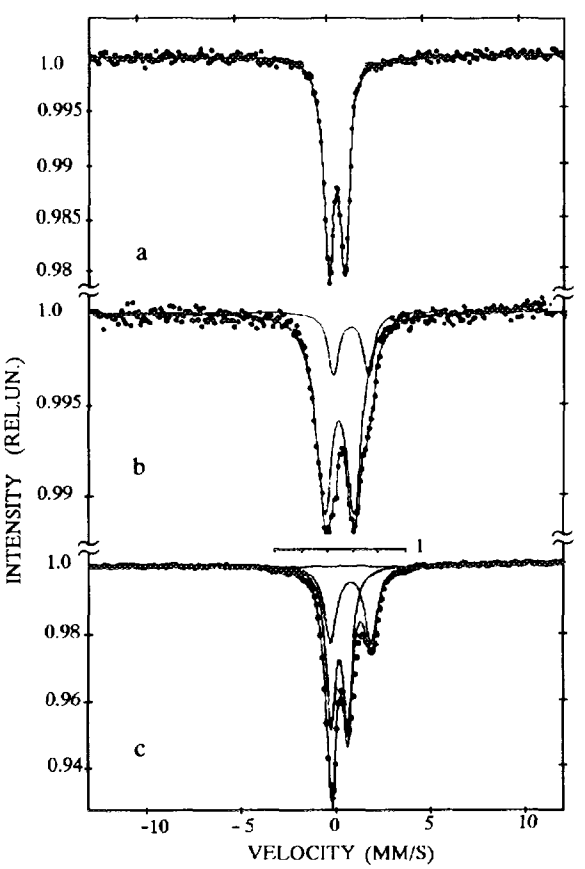

FIG. 4. Mössbauer spectra (T = 300 K) of the B–Zr catalyst activated by O_2 and H_2. (a) Gel, (b) gel after (O_2, H_2) activation, (c) (b) after CO hydrogenation.

carbide [17] and seem to be intermediate between ferrite (tetragonal martensite) and $Fe_{2-x}C$ carbide [18–20]. The presence of small magnetic clusters in the B–Zr catalyst is also supported by magnetic measurements (Fig. 2).

Role of Vacancies and Carbon Inclusions

Consider now the role of anion vacancies in catalyst activation and the participation of "oxidic" carbon [21] in carbide formation. Since the significant part of CO molecules is converted to CO_2 (Table 1), the direct synthesis of this product may be due to the reaction

$$CO + O_L \rightarrow CO_2 + V_L, \qquad [5]$$

where V_L is a newly formed active center. In accordance with [12] the $Fe^{3+}{=}O^{-2}$ terminal groups may well again participate in this reaction, as rigid conditions of CO hydrogenation will seem to favor electron–phonon excitation [22] with the breakage of the Fe–O bond. Thus, the anion vacancies may take part in CO disproportionation, i.e., the combination of (5) with the reaction

$$CO + V_L \rightarrow C_i + O_L, \qquad [6]$$

as well as the inverse Bell–Bouduar reaction, i.e., the combination of (2) and (6). Reaction (6) cures the nonstoichiometry defect, causing the creation of an active "oxidic" carbon.

Apart from the elementary steps (2), (5), and (6), the anion vacancies, when diffusing throughout the spinel, may segregate and form vacancy associations and zones of free volume. The thermally activated fluctuation of the composition, accompanied by vacancy ionization and electron transfer, may create in these zones the smallest metallic clusters, $[Fe^{(0)}]$, i.e., active intermediates and precursors of the metallic phase. It seems quite probable that these clusters have been observed in samples A and B during activation by H_2 (Fig. 2).

C_i participation may occur by three paths:

$$C_i \begin{cases} + H_2 \rightarrow [-CH_2-] \\ + C_i \rightarrow \text{coke} \\ + [Fe^{(0)}] \rightarrow \begin{cases} Fe_xC \\ \varepsilon\text{-}Fe_2C \\ \chi\text{-}Fe_5C_2 \end{cases} \end{cases}$$

An "oxidic" carbon may take part in hydrocarbon synthesis, in coke formation, and in reactions with $[Fe^{(0)}]$ intermediates. At low Fe concentrations the latter route yields small metastable carbide clusters (the cases of A, B, and B–Zr catalysts), while at higher Fe loadings (the case of C catalysts), the coalescence of the intermediates $[Fe^{(0)}]$ may compete with this reaction. Large metallic clusters produced by coalescence behave as volume metallic phases whose carburization yields large particles of χ-carbide.

The formation of metastable carbide clusters with $\langle d \rangle \approx 3$ nm appears to be a crucial point for process selectivity because only in the presence of such clusters do the highest yields of C_1–C_3–Ph and C_4–C_8–Ph occur. Modification by Zr causes the stabilization of the oxide matrix, inhibiting lattice oxygen mobility and vacancy formation and favoring the C_i reaction with iron intermediates.

The nature of the interface and the electronic exchange processes appear to be of great importance in establishing process selectivity. A more detailed description of this requires additional experimental data.

REFERENCES

1. Sinfelt, J. H., and Cusumano, J. A., *in* "Advanced Materials in Catalysis," (J. J. Burton and R. L. Garten, Eds.), p. 1. Academic Press, New York, 1977.
2. Knozinger, H., *in* "Catalysis by Acids and Bases" (B. Imelik *et al.*, Eds.), p. 111. Elsevier, New York, 1985.
3. Ollis, D. F., *J. Catal.* **23,** 131 (1971).
4. Freeman, M. J., Green, M., Orpen, A. G., Saltes, I. D., and Stone, F. G. A., *J. Chem. Soc., Chem. Commun.*, 1332 (1983).
5. Maksimov, Yu. V., Matveev, V. V., Suzdalev, I. P., *et al.*, Hyperfine Interact. **57,** 198 (1990).
6. Khomenko, T., Kadushin, A., Kutyreva, N., Maksimov, Yu., *et al.*, *J. Mol. Catal.* **51,** L9 (1989).
7. Khomenko, T., Kutyreva, N., Kadushin, A., Maksimov, Yu., *et al.*, *J. Mol. Catal.* **56,** 61 (1989).
8. Tsodikov, M. V., Ivanova, G. F., Bukhtenko, O. V., Ellert, O. G., Maksimov, Yu. V., and Zaslavskii, B. A., *Bull. Acad. Sci. USSR, Div. Chem. Sci. (Engl. Transl.)* **8,** 1898 (1988).
9. Maksimov, Yu. V., Matveev, V. V., Suzdalev, I. P., Tsodikov, M. V., and Ellert, O. G., *Hyperfine Interact.* **57,** 1983 (1990).
10. Tsodikov, M. V., Bukhtenko, O. V., Ellert, O. G., Markevich, V. V., Maksimov, Yu. V., and Loktev, S. M., *Bull. Acad. Sci. USSR, Div. Chem. Sci. (Engl. Transl.)* **2,** 295 (1991).
11. Deleted in proof.
12. Tsodikov, M. V., Kugel, V. Ya, Maksimov, Yu. V., *et al.*, *J. Catal.* **147,** (1994).
13. Schuit, G. C. A., and Gates, B. C., *AIChE J.* **19**(3), 417 (1973).
14. Yagnik, C. M., and Mathur, H. B., J. Phys. C: *Solid State Phys.* **1,** 469 (1968).
15. Morozova, O. S., Maksimov, Yu. V., Shashkin, D. P., *et al.*, *Appl. Catal.* **78,** 227 (1991).
16. Kroger, E. A., and Vink, H., Solid State Physics, **3,** 307 (1956).
17. Niemantsverdriet, J. W., Van der Kraan, A. M., Van Dijk, W. L., and Van der Baan, H. S., *J. Phys. Chem.* **84**(25), 3363 (1980).
18. Hofer, L. J. E., Cohn, E. M., and Peebles, W. C., *J. Am. Chem. Soc.* **71,** 189 (1949).
19. Barton, G. N., and Gale, B., *Acta Crystallogr.* **17,** 1460 (1964).
20. Ron, M., Shechter, H., and Niedzwieds, S., *J. Appl. Phys.* **39,** 265 (1968).
21. Krebs, H. J., Bonzel, H. P., and Gafner, G. A., *Surf. Sci.* **88**(1), 269 (1979).
22. Kazansky, V. B., Pershin, A. N., and Shelimov, B. N., *in* "Proceedings 7th International Congress on Catalysis, Tokyo, 1980" (T. Seiyama and K. Tanabe, Eds.), Vol. 1, p. 1210. Elsevier, Amsterdam, 1981.